Verification and possible applications of new 3D panel method with boundary layer

Vít Štorch*[1], Jiří Nožička[1]

[1] ČVUT v Praze, Fakulta strojní, Ústav mechaniky tekutin a termodynamiky, Technická 4, 166 07 Praha 6, Česká republika

Abstract

Robust and well tested 3D panel method for potential flow solution was coupled to a two-equation integral 2D boundary layer model. The result is a sophisticated tool for solving the problem of both steady and unsteady viscous flow around streamlined lifting bodies such as wings or blades of turbomachines in external flow. The key aspect of the model is a quasi-simultaneous computation using interaction coefficients that allow solution of boundary layer with transition and other regions of strong interaction. The advantages and shortcomings of the new model are discussed based on the comparison with CFD results and the results of an advanced lifting line model. An elliptic wing with NACA4415 airfoil was chosen as a test case for comparison. Drag evaluation in the Trefftz plane was used as an alternative method for drag calculation in order to minimize force over surface integration error.

Key-words: 3D panel method; Boundary layer coupling; Finite wing; CFD verification; Wing polar

1. Introduction

The use of finite volume methods for wide range of problems in fluid dynamics becomes more and more popular at the expense of other methods that were popular in the past. While the current commercial CFD packages give a meaningful and precise-enough answer for most type of flow problems, in some areas the versatility of the codes can actually lead to a less precise results compared to problem-specific numerical models. An example of such problem-specific analysis tool is the model described in this article, which is designed for flow around streamlined lifting bodies.

The presented numerical model was created as part of the project which aims to develop a new computational tool for contra-rotating propellers analysis. The model consist of a 3D panel method coupled to a 2D boundary layer solver. To establish the precision and reliability of the code, a simple validation problem of an external flow past a finite wing was proposed.

The 3D panel method was described previously by the author in [1] and the boundary layer model was described in [2]. A force-free wake is being shed from the trailing edge of the lifting body. Although the shape of the wake is not crucial for the case of finite wing, a robust wake model also used in contra-rotating propeller study [3] is attached to the finite wing. This paper presents a brief summary of the theory behind 3D panel method and boundary layer model but focuses mainly on the coupling of the methods together and on the verification process.

2. 3D panel method

Velocity formulation of panel method (also known as direct formulation, or Hess-type panel method) was used. Panel method solves the Laplace's elliptic partial differential equation:

$$\nabla^2\Phi = \Delta\Phi = \frac{\partial^2\Phi}{\partial x^2} + \frac{\partial^2\Phi}{\partial y^2} + \frac{\partial^2\Phi}{\partial z^2} = 0 \qquad (1)$$

Well known simple solutions of this equation exist, such as uniform flow, free vortex, source and doublet (dipole). By any superposition of these individual solutions, the Laplace's equation is satisfied automatically. What remains to be done is to ensure proper boundary condition definition and spatial distribution of elementary solutions before the computation can begin.

The boundary condition in case of velocity formulation is prescribed as zero flow through the body surface:

$$\vec{n} \cdot \vec{c} = 0 \qquad (2)$$

The surface of the body is discretized using quadrilateral panels of two types - constant source distribution panels and vortex ring panels. The boundary condition is evaluated in the midpoint of each panel (except wake panels). In theory, using only vortex ring panels type should be sufficient, however as found by trial and error, using both types of panels improves the solution considerably. The source strength σ is computed from the free stream velocity according to Ashby [4]:

$$\sigma = -\vec{n} \cdot \vec{c}_\infty \qquad (3)$$

Formulas for induced velocity of source panels were derived by Hess [5]. Vortex ring panel consisting of four vortex filaments positioned at the edge of the panel is equivalent to a constant doublet panel. An advantage of using vortex ring panels instead of doublet panels is easier implementation and the fact that the panels can be twisted. Formulas for induced velocity of a vortex ring panel and the proof of equivalency to constant doublet distribution panel can be found in [6].

*Corresponding author: Vit.Storch@fs.cvut.cz

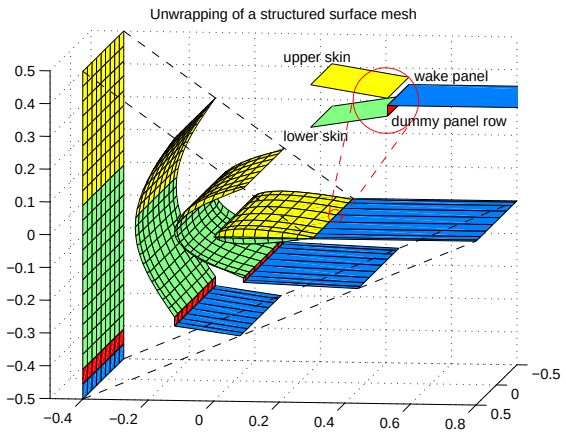

Fig. 1. *Structured surface mesh of a wing*

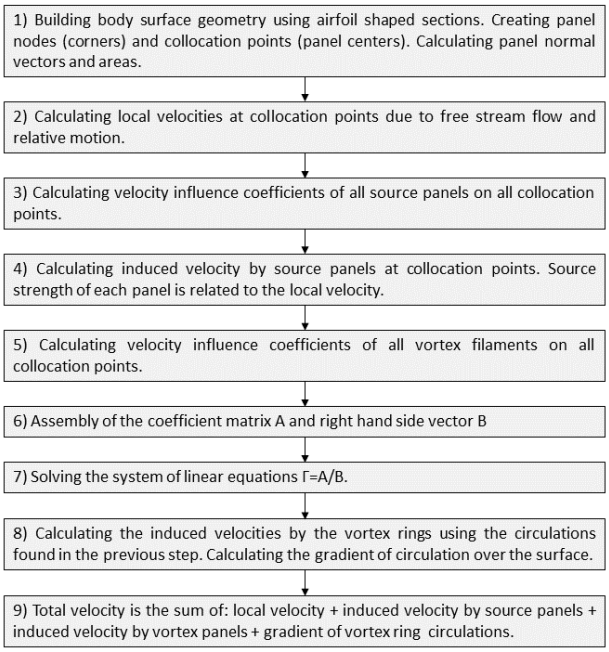

Fig. 2. *General iteration scheme of the unsteady solver for body under arbitrary rotation and translation*

The method uses structured mesh, which suits well for most cases such as wings and blades (see Fig. 1). There are M panel "columns" in spanwise direction and N panel rows in streamwise direction. Last two panel rows have special properties. Row $N-1$ is a dummy panel row, with zero induced velocities. Its only purpose is to allow a small trailing edge gap, which is often the case with many airfoil families. Panel row with index N is already outside of the body and serves as the first wake row. It doesn't have source component and the circulation of the vortex rings is set according to Kutta condition. The mesh data for each cell, such as midpoint and corner point coordinates, are stored in 2D matrix structures. This way the information about the neighboring cells necessary for surface gradient calculations are readily available from the data structure.

2.1. Steady calculation with frozen wake

There are two possible ways of using the 3D panel method. Either as a steady solver with frozen wake or an unsteady solver with force free wake. In case of frozen wake approach, the first row of wake panels is extended a significant distance behind the wing and no additional wake panels are added. The workflow of the solver is depicted in Fig. 2. No iteration is necessary.

When the system of equations is solved and all the unknown circulations are found, the last step remaining is to calculate the surface gradient of circulation:

$$\vec{c}_{\nabla\Gamma} = \frac{\nabla\Gamma}{2} \tag{4}$$

The resulting velocity at collocation points is calculated as a superposition of free stream velocity, velocity induced by source panels, by vortex rings and the surface gradient of circulation:

$$\vec{c} = \vec{c}_{\infty} + \vec{c}_{\sigma} + \vec{c}_{\Gamma} + \vec{c}_{\nabla\Gamma} \tag{5}$$

The first three components of the velocity already fulfill the boundary condition, the last member, gradient of circulation, only corrects the tangential velocity on the surface. No such correction is necessary in sufficient (at least one panel length) distance from the body and the first three components are used for off-body velocity calculation.

2.2. Unsteady solver with force free wake

Unsteady solver for K lifting bodies with force free wakes is an extension of the steady solver. The first wake panel row just behind the trailing edge is still frozen, but it is made very short. It is joined by the force free wake model, which is governed by a separate set of scripts. This way it is made "portable". The same wake model can be attached to the 3D panel body or to a simple lifting line model. The time stepping iteration scheme of the solver is shown in Fig. 3

For the purpose of the verification on the case of a finite wing, unsteady solver was chosen to verify that it produces reliable results with the force free wake.

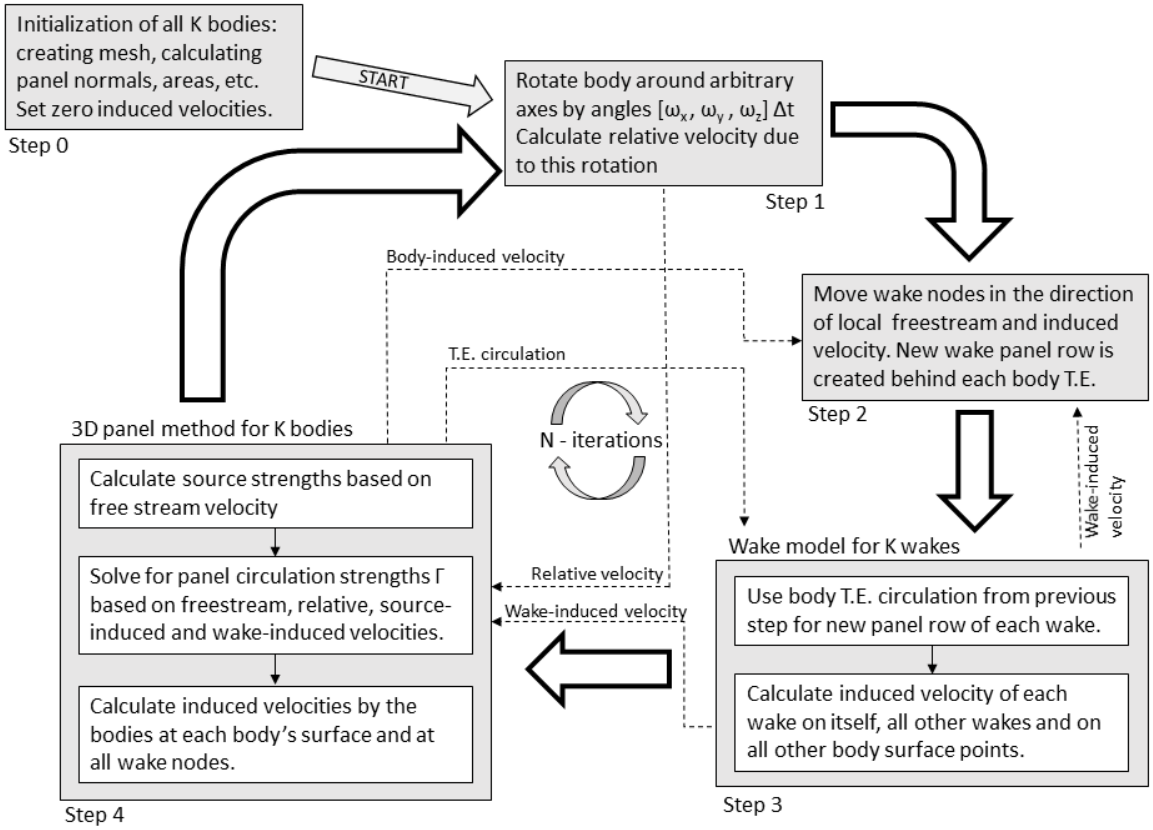

Fig. 3. *Iteration scheme of the unsteady solver for body under arbitrary rotation and translation*

3. 2D boundary layer model

The two equation integral boundary layer model used for this paper is described in detail in [2]. It is based mainly on the work of Drela [7],[8]. The first governing equation is the integral momentum equation:

$$\frac{d\theta}{d\xi} + (2+H)\frac{\theta}{u_e}\frac{du_e}{d\xi} = \frac{C_f}{2} \tag{6}$$

The second governing equation of the boundary layer model is the kinetic energy shape parameter equation:

$$\theta\frac{dH^*}{d\xi} + H^*(1-H)\frac{\theta}{u_e}\frac{du_e}{d\xi} = 2C_D - H^*\frac{C_f}{2} \tag{7}$$

The primary variables were chosen H and θ unlike the Drela's model where the primary variables are θ and δ^*. The edge velocity u_e depends on the the boundary layer displacement thickness and inviscid solution and is treated as a variable (see next section, coupling of the boundary layer). The remaining parameters of the boundary layer equation $H^* = H^*(H,\theta)$, $C_f = C_f(H,\theta)$ and $C_D = C_D(H,\theta)$ are defined by closure equations, which can be found in [7]. An auxiliary equation is solved together with the governing equations, which is different for turbulent and for laminar regions. In laminar region, it is the formula for perturbation amplification ratio $e^{\tilde{n}}$ leading to transition onset. It is based on the Orr-Sommerfeld equation, and is used in the following form:

$$\frac{d\tilde{n}}{d\xi} = \frac{d\tilde{n}}{dRe_\theta}\frac{m+1}{2}l\frac{1}{\theta} \tag{8}$$

Where:

$$\frac{d\tilde{n}}{dRe_\theta} = \frac{\sqrt{[2.4H - 3.7 + 2.5tanh(1.5H - 4.65)]^2 + 0.25}}{100} \tag{9}$$

$$l = \frac{6.54H - 14.07}{H^2} \tag{10}$$

$$m = \left(0.058\frac{(H-4)^2}{H-1} - 0.068\right)\frac{1}{l} \tag{11}$$

When $\tilde{n}$ reaches a predefined critical value $\tilde{n}_{crit}$ the solver switches to turbulent closure equations.

The auxiliary equation in turbulent region is that for shear stress coefficient. Green et al. [9] proposed a lag-entrainment method which estimates shear stress coefficient based on its equilibrium value:

$$\frac{\theta(3.15 + H + \frac{1.72}{H-1})}{C_\theta}\frac{dC_\tau}{d\xi} = 4.2(C_{\tau EQ}^{0.5} - C_\tau^{0.5}) \tag{12}$$

Where:

$$C_{\tau EQ} = H^*\frac{0.015(H-1)^3}{(1-U_s)H^3} \tag{13}$$

$$U_s = \frac{H^*}{2}\left(1 - \frac{4}{3}\frac{H-1}{H}\right) \tag{14}$$

3.1. Drag evaluation based on boundary layer properties

The far field viscous drag can be computed from the developed momentum thickness of the wake θ_∞ far downstream of the wing [10]:

$$D_{visc} = \varrho \theta_\infty c_\infty^2 \tag{15}$$

To avoid computing wake layer, Squire-Young formula is used, which extrapolates the behavior far downstream based on the state of boundary layer just behind the trailing edge.

$$D_{visc} = \varrho \theta_{T.E.} \left(\frac{c_{T.E.}}{c_\infty} \right)^{0.5(5+H_{T.E.})} c_\infty^2 \tag{16}$$

Where $c_{T.E.}$ is the inviscid velocity just behind the trailing edge (the edge velocity at trailing edge will be used) and $H_{T.E.}$ is the shape factor at the trailing edge. The total viscous drag is calculated as the sum of upper and lower boundary layer contributions.

4. Coupling of the boundary layer

Interaction between viscous boundary layer and inviscid panel method solution is the key element of the presented numerical method. The current form of interaction is based on the previous work regarding 2D flow past airfoils [2].

4.1. 2D case of interaction

In the aerodynamic tool XFOIL, the equations of boundary layer are solved together with the equations of inviscid 2D panel method. This way, the interaction between edge velocity u_e and displacement thickness δ^* is solved simultaneously. This approach brings difficulties in implementation of the solver, such as the necessity to solve the boundary layer on the same mesh as the inviscid solver. Moreover, implementation of such simultaneous solution for 3D panel method is not practical.

Current implementation is similar to the quasi-simultaneous interaction described by Veldman [11], however uses a different, newly developed interaction coefficient. During the downstream pass of the boundary layer solver, at every station the response of edge velocity to displacement thickness change must be known:

$$u_{e\,i,NEW} = u_{e\,i,OLD} + d_{ii} c_\infty (\delta^*_{i,NEW} - \delta^*_{i,OLD}) \tag{17}$$

A local linear interaction coefficient d_{ii} is calculated based on the inviscid solution:

$$d_{ii} = \frac{2 u_{e\,i,inv}}{c_\infty (\xi_i - \xi_{i-1})} \tag{18}$$

For more precise solution, several passes of the boundary layer with inviscid calculation in between can be performed. The implementation of the interaction coefficient has two benefits - the interaction prevents divergence of the solution in the regions of strong interaction, such as transition region, region of laminar bubbles and flow near trailing edge.

4.2. 3D case of interaction

First step of the boundary layer coupling algorithm is to calculate streamlines on the surface of the wing in inviscid flow. Arbitrary number of streamline emitting points can be specified at the stagnation line near the leading edge. Equal number of streamlines are calculated on the top and on the bottom surface. The inviscid surface velocity u_e and downstream coordinate ξ is then interpolated to obtain a higher number of stations. For a relatively quick and precise calculation using 3D panel method, about 30 streamwise panels are necessary to discretize the top and bottom of the airfoil. On the other hand, about 100 stations is required for each side of the airfoil for boundary layer calculation. Without the interpolation, the 3D panel method would have to use a prohibitive number of panels, since the computational time increases with the second power of the number of panels.

The input for the boundary layer calculator for each streamline are: the streamline coordinates, inviscid edge velocity, local interaction coefficient, density and kinematic viscosity of the fluid. The output of the BL solver is the skin friction coefficient and displacement thickness distributions along each streamline together with viscous drag estimation using the Squire-Young formula. The resulting parameters known only along each streamline are then extrapolated to the whole surface of the wing.

In the next step, the surface of the wing is displaced in the normal direction by the amount specified by extrapolated displacement thickness. After that the second calculation of inviscid flow past the modified body is carried out. This way the influence of inviscid flow on the boundary layer is captured by the local interaction coefficient, while the influence of boundary layer on the inviscid flow is captured by this second inviscid flow calculation using body enlarged by displacement thickness.

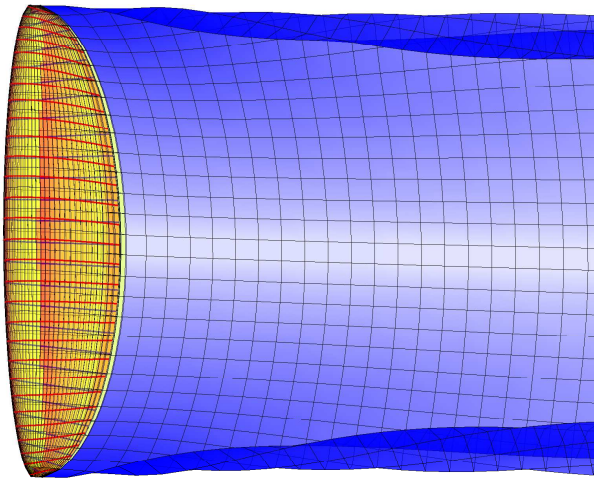

Fig. 4. *Streamlines on the top (red) and bottom (blue) surface.*

Important mechanism of separation is trailing edge separation, where the separation point moves forward with increasing angle of attack. The rapid growth of separated boundary layer behind the separation point causes lift reduction to the point of maximum lift. Without correct modeling of this phenomenon, lift near stall cannot be predicted realistically.

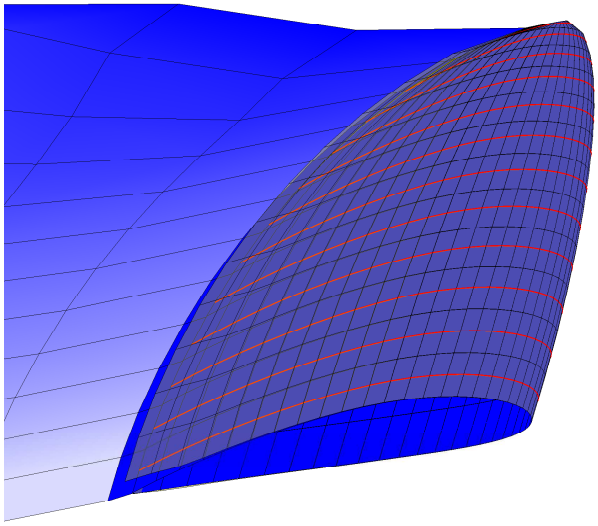

Fig. 5. *Trailing edge boundary layer separation*

5. Verification case of a finite wing

The comparison across numerical methods is performed using an elliptic finite wing as a model example (see Fig. 6). The wing is not twisted and uses NACA 4415 airfoil along the entire span. The root chord dimension is 1.25m and wingspan 5m, which provides relatively low aspect ratio of 5.11 and mean aerodynamic chord 0.98 m. Resulting Reynolds number $Re = 6 \cdot 10^5$ is in the lower region of range of interest of small aircraft propellers.

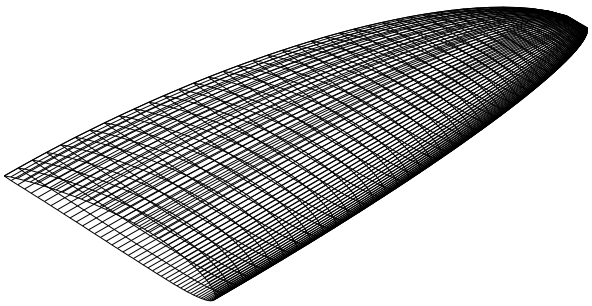

Fig. 6. *Surface mesh of the wing*

6. CFD calculation

To reduce computational time, only half of the wing is modeled with symmetry boundary condition. The computational domain is shown in Fig. 7. Velocity inlet and pressure outlet boundary condition are accompanied by standard no-slip condition on the surface of the wing.

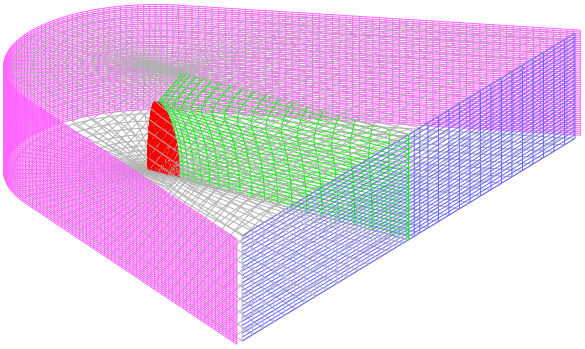

Fig. 7. *Overview of the domain with boundary conditions marked by different colors*

The volume mesh is a structured hexahedral mesh programmed and parametrized in MATLAB and exported directly to fluent .msh format using custom scripting. The wing is wrapped by a user specified number of inflation layers to allow different turbulence models. Two meshes were created, coarse mesh for $k - \epsilon$ turbulence model with 0.5 million cells, $y+ \approx 30$, and fine mesh for $k - \omega SST$ turbulence model with 2.2 million cells and $y+ \approx 3$. Side view of the coarse mesh is shown in figure 8. Detail of the coarse mesh is shown in figure 9.

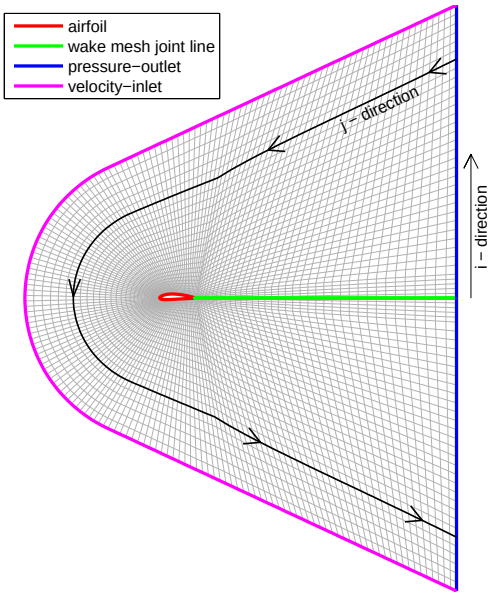

Fig. 8. *Side view of the coarse mesh*

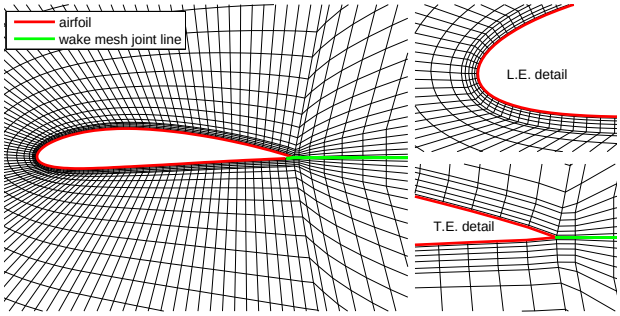

Fig. 9. *Detail of the coarse mesh near surface of the wing*

Three different turbulence models, $k-\epsilon$, $k-\omega SST$ and Transition $k-\omega SST$ were tested, last of which was considered to be the most appropriate for the relatively low Reynolds case with extensive laminar layer region. The remaining two models compute the whole boundary layer as turbulent. Inlet turbulence intensity and viscosity ratio were both set to the value 0.2.

6.1. Drag and lift evaluation

In case of CFD, lift is obtained by simple surface force integration. Drag, on the other hand, is known to be evaluated poorly from the surface integration, and wake inspecting methods usually produce more precise results.

Induced drag, as a byproduct of lift, can be calculated from the change of kinetic energy between front face of an imaginary bounding box aligned with the flow and its rear face (Trefftz plane) [6]:

$$D_i = -\frac{\varrho}{2}\int\int(c_y^2 + c_z^2)dydz \tag{19}$$

The remaining components of drag connected to viscosity (friction drag and pressure drag) can be expressed by a single viscous drag formula for incompressible flow [12]:

$$D_{visc} = \int\int \Delta p_0 dydz \tag{20}$$

Trefftz plane is positioned 5 mean aerodynamic chord lengths behind the wing in the CFD domain and oriented perpendicular to the inlet flow. The process of changing angle of attack, placing Trefftz plane and evaluating custom field functions is automated using journal script for FLUENT written by MATLAB.

7. Lifting line calculation

Lifting line calculation is based on the wing and wake representation by horseshoe vortices. Bound vortices are placed on the 1/4 chord length. Although not necessary, force-free wake is used instead of a simpler frozen wake model.

Before the calculation, NACA4415 polars are calculated for a whole range of Reynolds numbers and sufficient angle of attack range. Although the wing operates at overall Reynolds number 600 000, the Reynolds number at root section is slightly higher, and at tip section considerably lower. During iteration, the induced velocity together with free stream velocity produce effective angle of attack for each span section. Resulting local lift coefficient is then used for determining the local circulation of the bound vortex. Around 20 iterations are sufficient for convergence.

Evaluation of lift and drag is performed simply as the sum of contributions from each span station. It is important to rotate the local lift and drag vectors by the induced downwash angle, in order to obtain correct induced drag values.

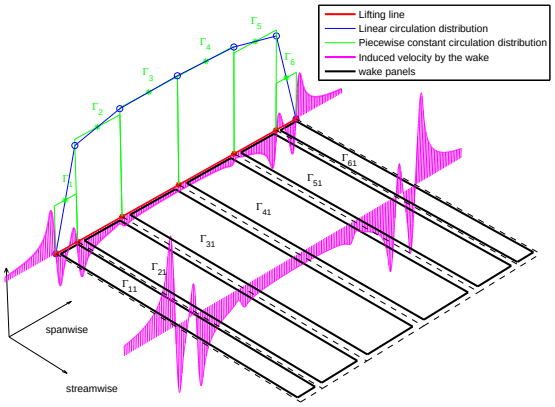

Fig. 10. *Topology of a simple lifting line model connected to a force free wake*

8. Results

Drag polar (c_l vs. c_d), lift coefficient vs. angle of attack (c_l vs. α) and c_d vs. α were analyzed to evaluate the performance of the computational models. Only one of the FLUENT's turbulence models was selected for comparison.

8.1. 3D panel method results

The 3D panel method with boundary layer uses in this example a surface mesh containing 60×30 panels for inviscid solution and total of 60 streamlines for boundary layer computation. Each streamline was discretized by 120 stations. The results are shown in the comparison section.

8.2. Cfd simulation results

All three turbulence models produced very similar polar curves (Fig. 11,12,13) between angles of attack $\alpha = -10°$ and $\alpha = 15°$. Transition SST model provides in this region more optimistic values of both lift and drag, due to laminar region of boundary layer, however the difference is barely noticeable. What is more noticeable is the discrepancy between total drag calculated by force integration and by Trefftz plane evaluation. Force integration is known to introduce high error to drag values, whereas Trefftz plane analysis in this case produces very low drag values. This could be linked to numerical dissipation error, since the Trefftz plane method relies on the correct modeling of dissipation in wake region.

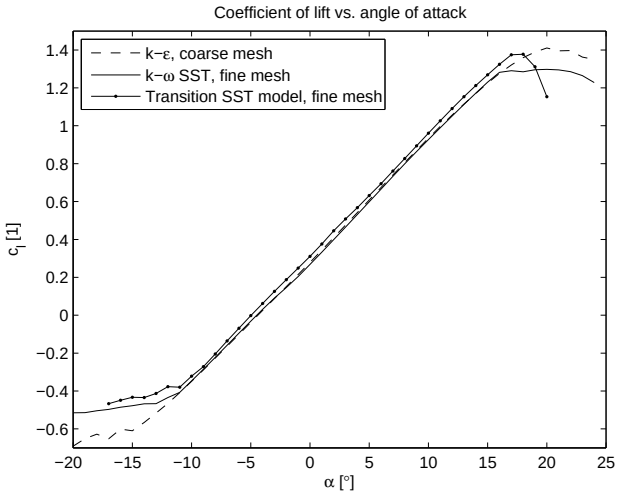

Fig. 11. *CFD: Coefficient of lift of the wing vs. angle of attack*

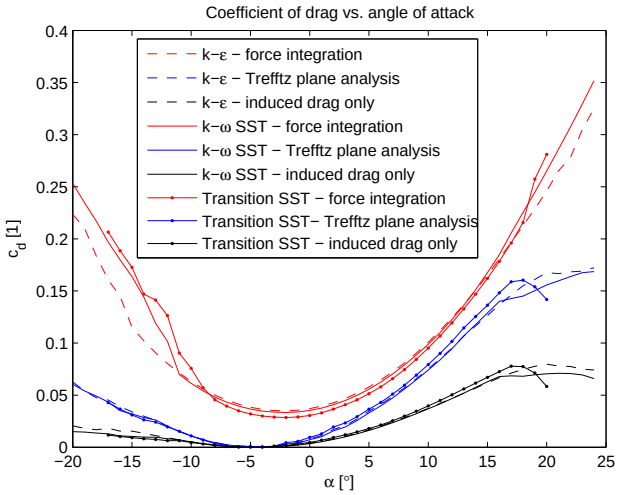

Fig. 12. *CFD: Coefficient of total drag and induced drag of the wing vs. angle of attack*

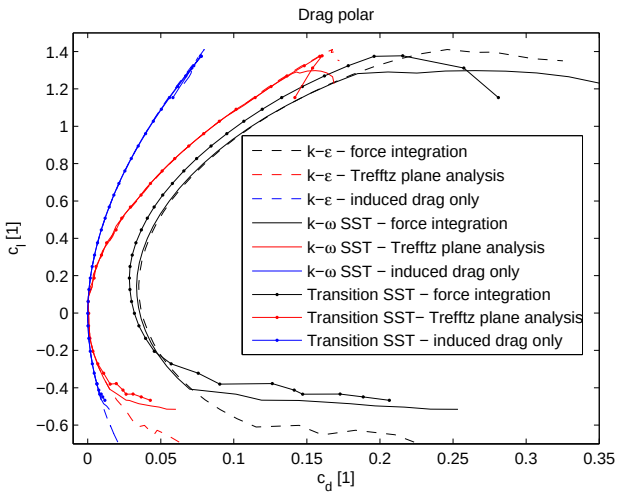

Fig. 13. *CFD: Total drag polar, induced drag polar*

For angles of attack higher than $\alpha = 15°$ or lower than $\alpha = -10°$ the turbulence models differ due to different prediction of separation. Because $k-\omega SST$ turbulence models are known to handle well regions with adverse pressure gradients, and because the case being analyzed has a considerable length of laminar boundary layer, Transition SST model was chosen for comparison with other computational models.

8.3. Lifting line method results

The solution using lifting line is very effective and straight-forward. The only problematic part is the last few percent of the wing span which have very small chord and low Reynolds numbers due to elliptic shape. The Reynolds number was limited by 100 000 from below, to overcome difficulties with calculating very low Reynolds number 2D airfoil polars. The results are presented below in the comparison section.

8.4. Comparison

The comparison of lift coefficient vs. α is in Fig. 14. As can be seen, the 3D panel method follows the results of lifting line model up to $\alpha = 8°$, where it changes abruptly slope and approaches the CFD solution. For negative angles of attack, CFD model predicts stall at $\alpha \approx -10°$ while both liffitng line model and 3D panel method results suggest attached flow.

Drag vs. angle of attack comparison in fig. 15 shows weaker agreement of the methods as could be anticipated. If the drag from force intergration of CFD results is disregarded, the results of the panel method fall between the drag computed by CFD Trefftz plane analysis and the lifting line results. The drag polar combining the drag and lift coefficients is presented in Fig. 16.

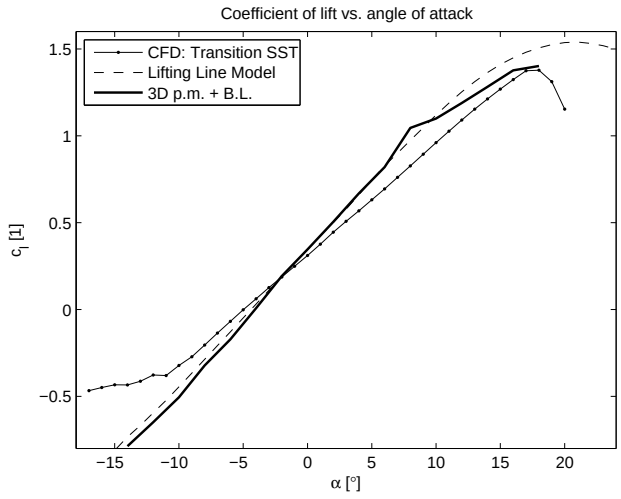

Fig. 14. *Coefficient of lift of the wing vs. angle of attack (Note: CFD = Transition SST model)*

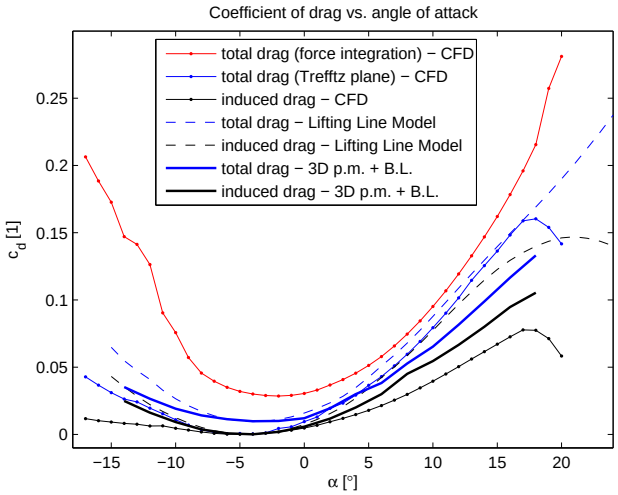

Fig. 15. *Coefficient of total drag and induced drag of the wing vs. angle of attack (Note: CFD = Transition SST model)*

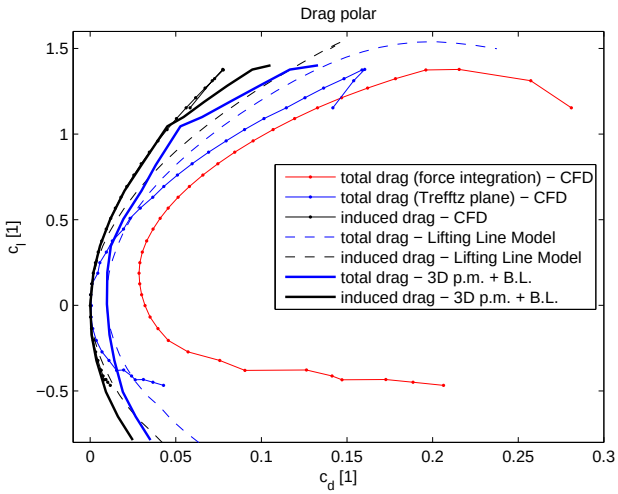

Fig. 16. *CFD: Total drag polar, induced drag polar*

9. Strenghts and weaknesses of the computational models

Based on the present and past experience with the three computational models, their performance is summarized in table 1. Different aspects of the models can be improved, for example accurate drag prediction using commercial finite volume CFD methods is possible, however it requires careful and precise mesh, turbulence model and domain fine-tuning.

Table 1. *Properties of computational models*

Model	3D panel method with BL	CFD, Transition SST	Lifting line
Polar generation time	≈ 10 min.	≈ 12 hr.	≈ 30 sec.
Lift prediction	good	good	good
Drag prediction	aceptable	poor	good
Moment prediction	good	good	not possible
Induced drag prediction	good	good	good
Transition modeling	implemented	implemented	2D polar dependent
Separation prediction	not reliable	good	acceptable
Complex geometry analysis	(mostly) suitable	suitable	not suitable
Optimization usability	very useful	limited (time consuming)	Perfect for simple wings

The advantages and disadvantages of the CFD solver and lifting line model are generally known. The presented 3D panel method with boundary layer coupling is an intermediate method regarding both its abilities and the need for computational resources. The method recognizes conditions of separation and simulates thick separated layers, however the polar curves show some inconsistent behavior in the regions of $c_{l,max}$.

9.1. Possible applications of the 3D panel method with boundary layer

The presented method was developed for strongly unsteady flow in contra-rotating propellers. Unlike in finite volume methods, where the domain required for computation of contra-rotating propellers is very complex, the presented model is capable of unsteady calculation without any additional modification. In fact, the results presented in this paper are calculated using unsteady sudden motion of the wing, with starting vortex in a sufficient distance from the wing. To obtain the solution for oscillating or rotating wing (blade), only the function prescribing rotation angle with time needs to be added. As an example, the top view of an oscillating wing with significant side slip angle is shown in Fig. 17.

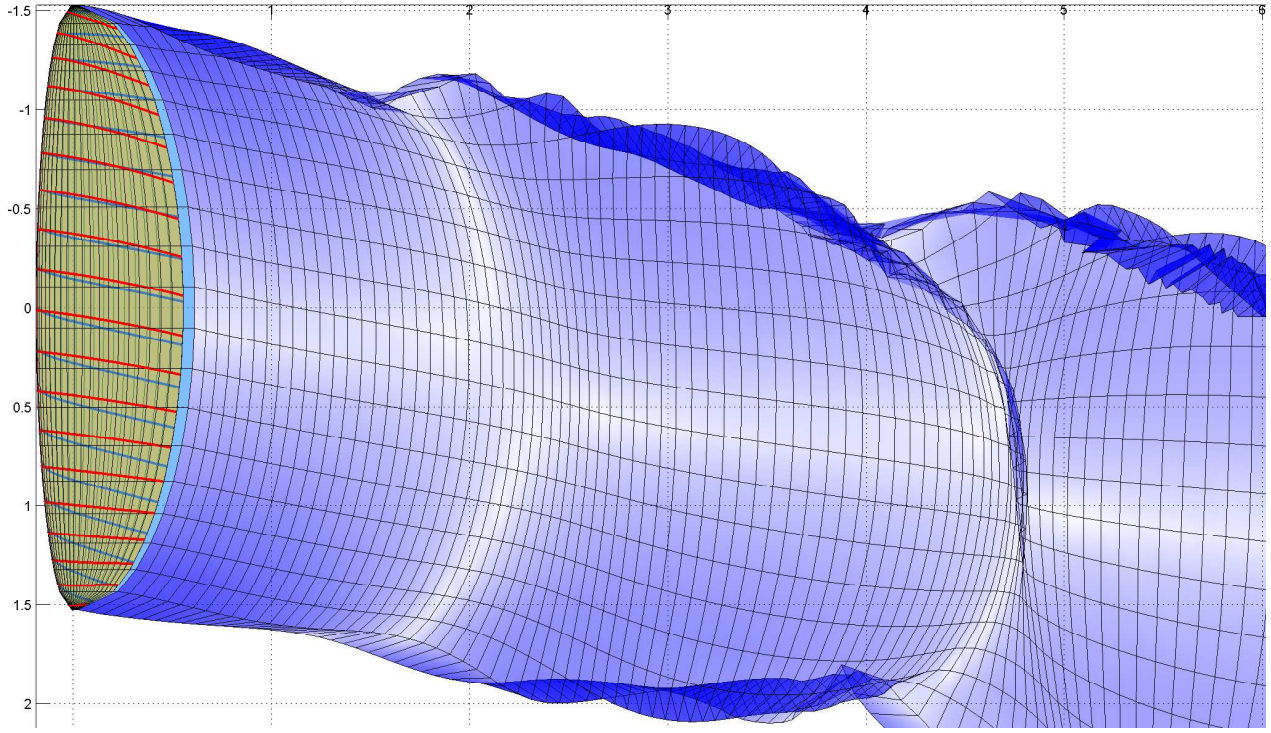

Fig. 17. *Wake behind oscillating and side slipping wing*

10. Conclusions

A 3D panel method coupled with boundary layer solver for incompressible low Reynolds number flow was briefly presented together with the underlying theory. The accuracy of the method is dependent on the coupling between viscous and inviscid model. For the purpose of quasi-simultaneous solution, new local linear interaction coefficient was introduced. The boundary layer thickness influences considerably the inviscid solution from moderate to high angles of attack. The method was tested on the case of an elliptic wing equipped with NACA 4415 airfoil. It retains good accuracy up to angles of attack near stall, but the behavior of parameters beyond stall is handled better by finite volume solvers.

Although the primary aim of the method is to simulate rotating blades of contra-rotating propellers, its application to other flow problems, such as optimization of wings or blades, is possible. One of the benefits is the computational speed, which is close to the very simple lifting line method.

The aim of future work is to improve the current simplified model of separation by modifying the behaviour of the boundary layer near the trailing edge. Next step is to apply the method on the case of contra rotating propellers and compare the results with experimental data from research that is already being conducted.

Acknowledgement

This work was supported by the Grant Agency of the Czech Technical University in Prague, grant No. SGS16/068/OHK2/1T/12

Nomenclature

$\vec{c}$	flow velocity vector	$(\mathrm{m}\cdot\mathrm{s}^{-1})$
C_D	dissipation coefficient	(1)
c_d	drag coefficient of wing	(1)
C_f	skin friction coefficient	(1)
c_l	lift coefficient of wing	(1)
C_τ	shear stress coefficient	(1)
$C_{\tau EQ}$	equilibrium shear stress coefficient	(1)
D	drag force	(N)
D_i	induced drag force	(N)
D_visc	viscous drag force	(N)
d_{ii}	interaction coefficient	(m^{-1})
H	shape parameter	(1)
H^*	kinetic energy shape p	(1)
L	lift force	(N)
M	number of spanwise panels	(1)
N	number of streamwise panels	(1)
$\vec{n}$	normal vector	(1)
$\tilde{n}$	TS wave amplification exponent	(1)
p_0	Total pressure	(Pa)
Re	Reynolds number	(1)
Re_θ	momentum thickness Reynolds number	(1)
t	time	(s)
u_e	BL edge velocity	(ms^{-1})
x, y, z	space coordinates	(m)
$y+$	dimensionless wall distance	(1)
α	angle of attack	(°)
Γ	circulation of a vortex filament	$(\mathrm{m}^2\mathrm{s}^{-1})$
δ^*	displacement thickness	(m)
θ	momentum thickness	(m)
ξ	BL surface coordinate	(m)
ϱ	density	$(\mathrm{kg}\cdot\mathrm{m}^{-3})$
σ	source strength density	(s^{-1})
Φ	Potential	$(\mathrm{m}^2\mathrm{s}^{-1})$

References

[1] V. Štorch and J. Nožička. "3D panel methods for turbomachinery design". In: *Studentská tvůrčí činnost 2014*. CTU in Prague, Faculty of Mechanical Engineering, 2014.

[2] V. Štorch and J. Nožička. "On viscous-inviscid interaction for boundary layer calculation using two-equation integral method". In: *Studentská tvůrčí činnost 2015*. CTU in Prague, Faculty of Mechanical Engineering, 2015.

[3] V. Štorch and J. Nožička. "A novel computational model for the analysis of contra-rotating propellers". In: *Studentská tvůrčí činnost 2016*. CTU in Prague, Faculty of Mechanical Engineering, 2016.

[4] D. Ashby. *Potential flow theory and operation guide for the panel code PMARC_14*. TM-1999-209582. NASA, Ames Research Center. Moffet Field, CA, 1999.

[5] A. Smith and J. Hess. *Calculation of non-lifting potential flow about arbitrary three-dimensional bodies*. Tech. rep. E.S. 40622. Long Beach, CA: Douglas Aircraft Company, Inc., 1962.

[6] J. Katz and A. Plotkin. *Low-Speed Aerodynamics*. Cambridge Aerospace Series. Cambridge University Press, 2001. ISBN: 9780521665520.

[7] M . Drela and M. Giles. "Viscous-Inviscid Analysis of Transonic and Low Reynolds Number Airfoils". In: *AIAA Journal* 25.10 (1987), pp. 1347–1355.

[8] M. Drela. "XFOIL – An analysis and design system for low Reynolds number airfoils". In: *Low Reynolds number aerodynamics* (1989).

[9] J. E. Green, D. Weeks, and J. Brooman. *Prediction of turbulent boundary layers and wakes in compressible flow by a lag-entrainment method*. London: H.M.S.O, 1977. ISBN: 9780114709624.

[10] R. Eppler. "About classical problems of airfoil drag". In: *Aerospace Science and Technology* 7.4 (2003), pp. 289–297.

[11] A. E. P. Veldman. "New, quasi-simultaneous method to calculate interacting boundary layers". In: *AIAA Journal* 19.1 (1981), pp. 79–85.

[12] M. B. Giles and R. M. Cummings. "Wake Integration for Three-Dimensional Flowfield Computations: Theoretical Development". In: *Journal of Aircraft* 36.2 (1999), pp. 357–365.